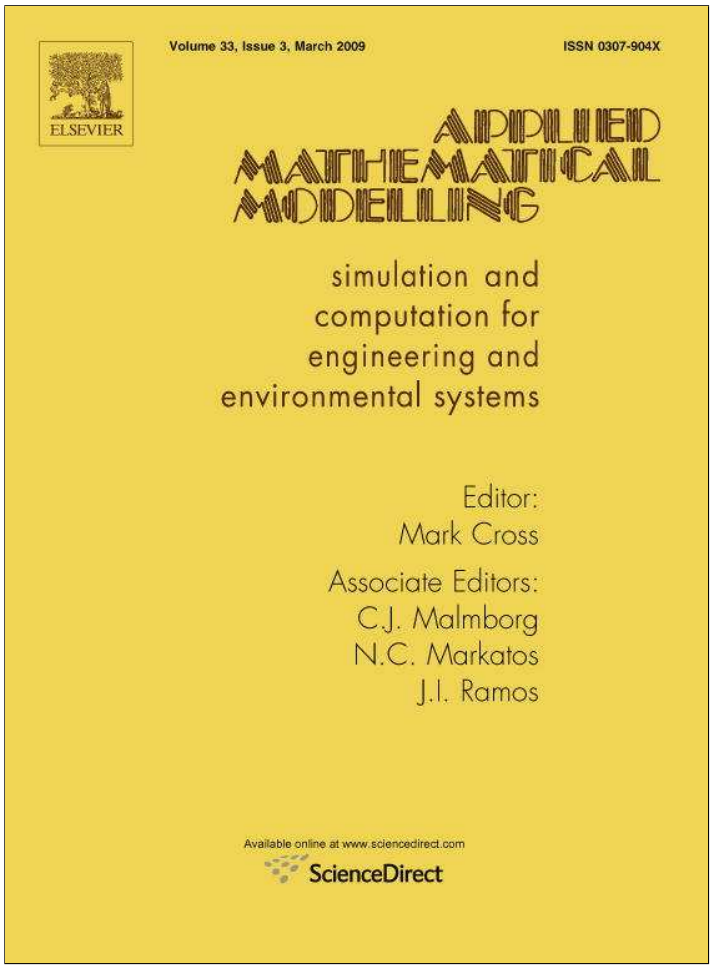

Applied Mathematical Modelling 33 (2009) 1776–1792

Contents lists available at ScienceDirect

Applied Mathematical Modelling

journal homepage: www.elsevier.com/locate/apm

Evaluation of the stress singularities of plane V-notches in bonded dissimilar materials

Zhongrong Niu [a,*], Dali Ge [a], Changzheng Cheng [a], Jianqiao Ye [a,b], Naman Recho [c]

[a] School of Civil Engineering, Hefei University of Technology, Hefei 230009, PR China
[b] School of Civil Engineering, The University of Leeds, Leeds LS2 9JT, UK
[c] Institute JLRA – CNRS UMR 7190, University P. and M. Curie-Paris VI, 75005 Paris, France

ARTICLE INFO

Article history:
Received 27 July 2007
Received in revised form 16 March 2008
Accepted 25 March 2008
Available online 1 April 2008

Keywords:
Stress singularity orders
Ordinary differential equations (ODEs)
The interpolating matrix method
V-notch
Bonded dissimilar materials
Orthotropic material

ABSTRACT

According to the linear theory of elasticity, there exists a combination of different orders of stress singularity at a V-notch tip of bonded dissimilar materials. The singularity reflects a strong stress concentration near the sharp V-notches. In this paper, a new way is proposed in order to determine the orders of singularity for two-dimensional V-notch problems. Firstly, on the basis of an asymptotic stress field in terms of radial coordinates at the V-notch tip, the governing equations of the elastic theory are transformed into an eigenvalue problem of ordinary differential equations (ODEs) with respect to the circumferential coordinate θ around the notch tip. Then the interpolating matrix method established by the first author is further developed to solve the general eigenvalue problem. Hence, the singularity orders of the V-notch problem are determined through solving the corresponding ODEs by means of the interpolating matrix method. Meanwhile, the associated eigenvectors of the displacement and stress fields near the V-notches are also obtained. These functions are essential in calculating the amplitude of the stress field described as generalized stress intensity factors of the V-notches. The present method is also available to deal with the plane V-notch problems in bonded orthotropic multi-material. Finally, numerical examples are presented to illustrate the accuracy and the effectiveness of the method.

1. Introduction

Recently, the development of the theory of fiber reinforced polymer (FRP) composite materials has been further motivated from strengthening and repairing various engineering structures. The cases of V-notches of bonded dissimilar materials are frequently encountered in engineering applications. In such cases, there exists strong stress concentration near the sharp notch and interface end. In particular, the peak stress at the notch tip is singular according to the theory of elasticity and depends on the geometrical configuration and material properties of the notch. Fatigue failure of the structures usually occurs starting from a notch tip.

For a V-notch of homogeneous elastic body with opening angle α, as shown in Fig. 1, the singular stress field near the V-notch tip can be expressed as a series expansion with respect to the radial coordinate in the following form [1–6]:

$$\sigma_{ij} = A\rho^{\lambda}\tilde{\sigma}_{ij}(\theta), \tag{1}$$

* Corresponding author. Tel.: +86 551 2901437; fax: +86 551 2902066.
E-mail address: niu-zr@hfut.edu.cn (Z. Niu).

S0307-904X/$ - see front matter © 2008 Elsevier Inc. All rights reserved.
doi:10.1016/j.apm.2008.03.007

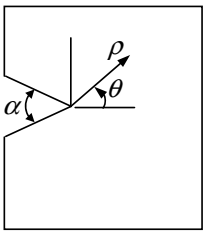

Fig. 1. A V-notch with opening angle α.

where the exponent λ is called stress singularity order, $\tilde{\sigma}_{ij}(\theta)$ are the associated eigenfunctions, A is the coefficient of the asymptopic expansion (called the generalized stress intensity factor). To study the singularity of the isotropic elastic V-notch, Williams [1] established the characteristic equation by using the Airy stress function method, as follows:

$$f(\lambda) = \pm\lambda \sin\beta + \sin(\lambda\beta) = 0, \tag{2}$$

where $\beta = 2\pi - \alpha$. It can be seen that the exponent λ depends on the opening angle α. The smallest real position roots λ generally satisfy $\lambda \in (-1,0)$ in the case $\alpha < \pi$.

The two key aspects of solving a V-notch problem in linear elasticity are to determine stress singularities and then find the associated amplitudes of the stress field that usually denoted as the generalized stress intensity factors of the V-notch tip. In a general case of V-notch, the exponent λ may be real or complex.

Various methods have been proposed to treat V-notch problems. Gross et al. [7,8] and Carpenter [9] obtained the generalized stress intensity factors for plane V-notch problems by a boundary collocation method. Boundary element method was also used to solve the displacement and stress fields of plane V-notch problems [10,11]. In the last decade, significant more work has been done to study V-notch problems because of an increased use of coatings and composite structures. Using Eq. (2) as a starting point, the sub-region accelerated Müller method [12] was utilized to compute the eigenvalues of the stress field near V-notch tips. The algebraic equation system in terms of unknown parameters in the analytical expression of the stress field was derived by the sub-region mixed energy principle, by which the stress amplitudes were also calculated. Jian et al. [13] evaluated the stress exponents of V-notches made of bonded bimaterial, using a complex potential theory and Newton's iteration method. The stress amplitudes were then obtained in conjunction with the use of hybrid finite element. Gadi et al. [14] derived the analytical formulations of thermally induced logarithmic stress singularities in a composite wedge composed of incompressible materials. Through using the state space method for a plane notch formed from several bonded anisotropic materials, Li et al. [15] established a governing eigenequation according to the elasticity theory, which can provide the stress singularity orders of the V-notches by means of an iteration technique for roots finding. By applying the Lekhnitskii formalism and Stroh formalism [16], Ting [17] studied the solutions of the stress fields of general anisotropic elastic materials and composites, in which the explicit expressions of the stress functions of some cases were presented as the form of a sextic equation. With the same way, the study of stress singularities at the tip of a V-notch that consists of an arbitrary number of dissimilar anisotropic elastic wedges was given by Ting [18]. After then, Hwu et al. [19] deduced an explicit closed-form eigenequation for determining the singular order near the anisotropic elastic composite wedge apex. Since the singular orders λ appear in the eigenequation as some nonlinear forms, an iteration technique should be needed to search the solutions of the singular orders from the associated determinant of the eigenequation for general V-notch problems. With the solutions of stress singularities, Labossiere and Dunn [20] and Hwu and Kuo [21] computed the stress intensity factors through the near tip displacement and stress fields from the conventional finite element analysis as well as the calculation of the path-independent H-integral [22]. Chue and Liu [23], Wigger and Becker [24] obtained the eigenequations of the plane anisotropic wedges by using Lekhnitskii's complex function method, which were used to calculate the stress singularity orders. Sue et al. [25] used complex potential function and eigenfunction expansion method to determine the stress singularity order of a magnetoelectroelastic bonded antiplane wedge.

The above mentioned research works are difficult to find the associated eigenfunctions $\tilde{\sigma}_{ij}(\theta)$ related to multiple singularity orders of the V-notches. It is naturally considered that the conventional finite element method and boundary element method can model the singular stress field by increasing the mesh density in the notch tip region. Unfortunately, the improvement on the accuracy of the approaches is very limited in comparison with increasing a large amount of the computation time. Recently, a special finite element method was used to deal with some V-notch problems based on the assumption of asymptotic expansion of the stress field near V-notch tips. For the V-notch and line crack shown in Fig. 1, Seweryn [26] taken two or three leading terms of the asymptotic expansion in Eq. (1) as the analytical constrains of stress field in the notch tip region. Then the analytical elements are applied in order to model the stress field in the core region around the singular tip. The remaining area of the structure can be modeled using the conventional finite elements. The approach can provide two or three singular exponents and stress amplitudes. It should be noted that the way need to know the analytical constrains like $\tilde{\sigma}_{ij}(\theta)$ in Eq. (1) before evaluating the singular exponent and stress field around the notch tip. Three leading terms of the analytical constrains were found only in the case of homogeneous isotropic crack [2]. However, the analytical constrains are difficult to be found prior to the evaluation of the stress singularity order of general V-notch problems of bonded dissimilar multi-material. Hence some approximate constrain functions $\tilde{\sigma}_{ij}(\theta)$ are proposed to support the way.

According to the idea, Carpinteri et al. [27] calculated the first leading singular exponent and mode I stress amplitude for the multi-layered beam with a crack or re-entrant corner symmetrically meeting a bimaterial interface with the finite element method. Chen and Sze [3] proposed a new eigenanalysis method with hybrid finite element and the assumption of asymptotic expansion to determine the stress exponents and stress amplitudes of bonded bimaterial V-notches.

The aim of this paper is to study the stress singularities of plane V-notch problems of bonded dissimilar materials. The governing equations of linear elasticity are transformed to eigenvalue problems of ordinary differential equations (ODEs) based on the assumption that the stress fields are asymptotic near the V-notch tips. The first author [28] established the interpolating matrix method to solve two-point boundary value problems of ODEs. The method is further developed in the present work to analyze eigenvalue problems of ODEs. As an application, the stress singularity orders and the associated eigenvectors are obtained by applying the interpolating matrix method to the ODEs of V-notches.

2. The eigenvalue problems of ODEs for plane V-notches in linear elasticity

Firstly, let us consider a V-notch of isotropic material with opening angle $2\pi - \theta_1 - \theta_2$ as shown in Fig. 2. Define a polar coordinate system (ρ, θ), taking the notch tip as origin. In the linearly elastic analysis, it has been verified that the displacement field in the notch tip region can be expressed as a series expansion with respect to the radial coordinate ρ originating from the notch tip [4]. One typical term of the series can be written in the following form:

$$u_\rho(\rho,\theta) = \rho^{\lambda+1}\tilde{u}_\rho(\theta), \tag{3a}$$

$$u_\theta(\rho,\theta) = \rho^{\lambda+1}\tilde{u}_\theta(\theta), \tag{3b}$$

where $\lambda, \tilde{u}_\rho(\theta)$ and $\tilde{u}_\theta(\theta)$ are eigenpairs. Introducing Eq. (3) into the strain–displacement relations of linearly elastic theory yields the strain components as

$$\varepsilon_{\rho\rho} = (1+\lambda)\rho^\lambda\tilde{u}_\rho(\theta), \tag{4a}$$

$$\varepsilon_{\theta\theta} = \rho^\lambda\tilde{u}_\rho(\theta) + \rho^\lambda\tilde{u}'_\theta(\theta), \tag{4b}$$

$$\gamma_{\rho\theta} = \rho^\lambda\tilde{u}'_\rho(\theta) + \lambda\rho^\lambda\tilde{u}_\theta(\theta), \tag{4c}$$

where $(\cdots)' = d(\cdots)/d\theta$. From linearly elastic behavior law (Hooke's law) of plane stress problems, the plane stresses are expressed as

$$\sigma_{\rho\rho} = \frac{E}{1-\nu^2}\rho^\lambda[(1+\lambda)\tilde{u}_\rho + \nu\tilde{u}_\rho + \nu\tilde{u}'_\theta], \tag{5a}$$

$$\sigma_{\theta\theta} = \frac{E}{1-\nu^2}\rho^\lambda[(1+\lambda)\nu\tilde{u}_\rho + \tilde{u}_\rho + \tilde{u}'_\theta], \tag{5b}$$

$$\sigma_{\rho\theta} = \frac{E}{2(1+\nu)}\rho^\lambda(\lambda\tilde{u}_\theta + \tilde{u}'_\rho), \tag{5c}$$

where E is Young's modulus and ν, Poisson's ratio. Notice that the eigenpairs in Eq. (3) depend on the configurations (wedge angles), material properties and boundary conditions of the V-notches, which are not influenced by any load. Thus the body forces are neglected and then the equilibrium equations are

$$\frac{\partial\sigma_{\rho\rho}}{\partial\rho} + \frac{1}{\rho}\frac{\partial\sigma_{\rho\theta}}{\partial\theta} + \frac{\sigma_{\rho\rho}-\sigma_{\theta\theta}}{\rho} = 0, \tag{6a}$$

$$\frac{1}{\rho}\frac{\partial\sigma_{\theta\theta}}{\partial\theta} + \frac{\partial\sigma_{\rho\theta}}{\partial\rho} + \frac{2\sigma_{\rho\theta}}{\rho} = 0. \tag{6b}$$

Substituting Eq. (5) into Eq. (6) gives

$$\tilde{u}''_\rho + \left(\frac{1+\nu}{1-\nu}\lambda - 2\right)\tilde{u}'_\theta + \frac{2}{1-\nu}\lambda(\lambda+2)\tilde{u}_\rho = 0, \quad \theta\in(\theta_1,\theta_2), \tag{7a}$$

$$\tilde{u}''_\theta + \left[2 + \frac{1}{2}(1+\nu)\lambda\right]\tilde{u}'_\rho + \frac{1}{2}(1-\nu)\lambda(\lambda+2)\tilde{u}_\theta = 0, \quad \theta\in(\theta_1,\theta_2). \tag{7b}$$

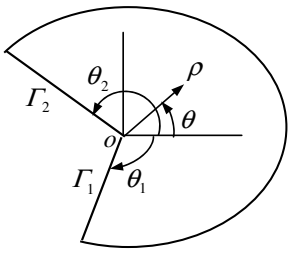

Fig. 2. Geometry near a V-notch.

Assume that all the tractions on the two edges, Γ_1 and Γ_2, near the notch tip are zero. That is

$$\left\{\begin{array}{c}\sigma_{\theta\theta}\\ \sigma_{\rho\theta}\end{array}\right\}_{\theta=\theta_1}=\left\{\begin{array}{c}\sigma_{\theta\theta}\\ \sigma_{\rho\theta}\end{array}\right\}_{\theta=\theta_2}=\left\{\begin{array}{c}0\\ 0\end{array}\right\}. \tag{8}$$

Hence, substitution of Eq. (5) into Eq. (8) yields

$$\tilde{u}'_\theta+(1+v+v\lambda)\tilde{u}_\rho=0,\quad \theta=\theta_1 \text{ and } \theta_2, \tag{9a}$$
$$\tilde{u}'_\rho+\lambda\tilde{u}_\theta=0,\quad \theta=\theta_1 \text{ and } \theta_2. \tag{9b}$$

Considering that the appearance of λ^2 in Eq. (7) leads to nonlinear eigenanalysis if Eq. (7) is directly solved, an alternative approach is adopted in this paper to transfer the equation into a linear eigenvalue problem. To this end, two new field variables are introduced as follows:

$$g_\rho(\theta)=\lambda\tilde{u}_\rho(\theta),\quad \theta\in(\theta_1,\theta_2), \tag{10a}$$
$$g_\theta(\theta)=\lambda\tilde{u}_\theta(\theta),\quad \theta\in(\theta_1,\theta_2). \tag{10b}$$

Thus, Eq. (10), Eq. (7) can been rewritten as

$$\tilde{u}''_\rho+\left(\frac{1+v}{1-v}\lambda-2\right)\tilde{u}'_\theta+\frac{2}{1-v}(\lambda+2)g_\rho=0,\quad \theta\in(\theta_1,\theta_2), \tag{11a}$$
$$\tilde{u}''_\theta+\left[2+\frac{1}{2}(1+v)\lambda\right]\tilde{u}'_\rho+\frac{1}{2}(1-v)(\lambda+2)g_\theta=0,\quad \theta\in(\theta_1,\theta_2). \tag{11b}$$

By following the above procedure, the evaluation of the singularity orders near a V-notch tip is transformed to solving a linear eigenvalue problem of the ODEs governed by Eqs. (10) and (11) subjected to the boundary condition of Eq. (9). In the solutions the associated eigenfunctions $\tilde{u}_\rho$ and $\tilde{u}_\theta$ can also be obtained and can be used to determine the stresses in the vicinity of the notch tip.

3. Evaluation of the stress singularities of V-notches of bonded dissimilar materials

Consider a V-notch problem of bonded bimaterial, as seen in Fig. 3. The body consists of two subdomains of different materials. E_1 and v_1 are, respectively, Young's modulus and Poisson's ratio of subdomain Ω_1, and E_2 and v_2 are ones of subdomain Ω_2. From the above derivation, it is obvious that Eqs. (10) and (11) are valid for each subdomain for analyzing the stress singularity orders near the interface tip of the dissimilar materials. Thus, the respective governing equations in the two subdomains are written as

$$\tilde{u}''_{1\rho}+\left(\frac{1+v_1}{1-v_1}\lambda-2\right)\tilde{u}'_{1\theta}+\frac{2}{1-v_1}(\lambda+2)g_{1\rho}=0,\quad \theta\in(\theta_1,\theta_2), \tag{12a}$$
$$\tilde{u}''_{1\theta}+\left[2+\frac{1}{2}(1+v_1)\lambda\right]\tilde{u}'_{1\rho}+\frac{1}{2}(1-v_1)(\lambda+2)g_{1\theta}=0,\quad \theta\in(\theta_1,\theta_2), \tag{12b}$$

$$g_{1\rho}(\theta)=\lambda\tilde{u}_{1\rho}(\theta),\quad \theta\in(\theta_1,\theta_2), \tag{13a}$$
$$g_{1\theta}(\theta)=\lambda\tilde{u}_{1\theta}(\theta),\quad \theta\in(\theta_1,\theta_2) \tag{13b}$$

and

$$\tilde{u}''_{2\rho}+\left(\frac{1+v_2}{1-v_2}\lambda-2\right)\tilde{u}'_{2\theta}+\frac{2}{1-v_2}(\lambda+2)g_{2\rho}=0,\quad \theta\in(\theta_2,\theta_3), \tag{14a}$$
$$\tilde{u}''_{2\theta}+\left[2+\frac{1}{2}(1+v_2)\lambda\right]\tilde{u}'_{2\rho}+\frac{1}{2}(1-v_2)(\lambda+2)g_{2\theta}=0,\quad \theta\in(\theta_2,\theta_3), \tag{14b}$$

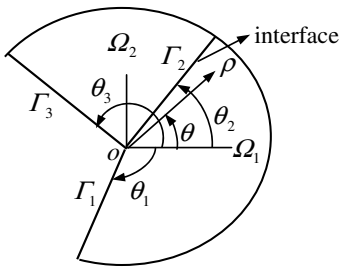

Fig. 3. A V-notch of bonded bimaterial.

$$g_{2\rho}(\theta) = \lambda \tilde{u}_{2\rho}(\theta), \quad \theta \in (\theta_2, \theta_3), \tag{15a}$$
$$g_{2\theta}(\theta) = \lambda \tilde{u}_{2\theta}(\theta), \quad \theta \in (\theta_2, \theta_3), \tag{15b}$$

where $\tilde{u}_{1\rho}(\theta), \tilde{u}_{1\theta}(\theta)$ are the eigenfunctions of displacement components in subdomain Ω_1 near the notch tip; $\tilde{u}_{2\rho}(\theta), \tilde{u}_{2\theta}(\theta)$ are the corresponding functions in subdomain Ω_2. For the bonded bimaterial, the continuity conditions of displacement components and the interface tractions must be satisfied on Γ_2, i.e.,

$$\tilde{u}_{1\rho}(\theta_2) = \tilde{u}_{2\rho}(\theta_2), \tag{16a}$$
$$\tilde{u}_{1\theta}(\theta_2) = \tilde{u}_{2\theta}(\theta_2) \tag{16b}$$

and

$$\left\{ \begin{array}{c} \sigma_{1\theta\theta} \\ \sigma_{1\rho\theta} \end{array} \right\}_{\theta=\theta_2} = \left\{ \begin{array}{c} \sigma_{2\theta\theta} \\ \sigma_{2\rho\theta} \end{array} \right\}_{\theta=\theta_2}. \tag{17}$$

Substitution of Eq. (5) into Eq. (17) gives

$$\frac{E_1}{1-\nu_1^2}[\tilde{u}'_{1\theta} + (1+\nu_1+\nu_1\lambda)\tilde{u}_{1\rho}] - \frac{E_2}{1-\nu_2^2}[\tilde{u}'_{2\theta} + (1+\nu_2+\nu_2\lambda)\tilde{u}_{2\rho}] = 0, \quad \theta = \theta_2, \tag{18a}$$
$$\frac{E_1}{2(1+\nu_1)}(\tilde{u}'_{1\rho} + \lambda\tilde{u}_{1\theta}) - \frac{E_2}{2(1+\nu_2)}(\tilde{u}'_{2\rho} + \lambda\tilde{u}_{2\theta}) = 0, \quad \theta = \theta_2. \tag{18b}$$

Similar to Eq. (9), applying the traction-free boundary conditions on Γ_1 and Γ_3 yields

$$\tilde{u}'_{1\theta} + (1+\nu_1+\nu_1\lambda)\tilde{u}_{1\rho} = 0, \quad \theta = \theta_1, \tag{19a}$$
$$\tilde{u}'_{1\rho} + \lambda\tilde{u}_{1\theta} = 0, \quad \theta = \theta_1, \tag{19b}$$

$$\tilde{u}'_{2\theta} + (1+\nu_2+\nu_2\lambda)\tilde{u}_{2\rho} = 0, \quad \theta = \theta_3, \tag{20a}$$
$$\tilde{u}'_{2\rho} + \lambda\tilde{u}_{2\theta} = 0, \quad \theta = \theta_3. \tag{20b}$$

Thus, the evaluation of the singularity orders λ near the V-notch tip of bonded bimaterial has been transformed into solving ODEs Eqs. (12)–(15) subjected to boundary conditions Eqs. (16), (18)–(20).

4. Evaluation of the stress singularities of V-notches of orthotropic materials

Consider a plane V-notch problem of orthotropic material, as seen in Fig. 4. Two principal axes of the orthotropic material are denoted Axes 1 and 2, respectively. θ_0 is the angle between Axis 1 and x-direction of the Cartesian coordinate system oxy. $o\rho\theta$ is a polar coordinate system where the notch tip is the pole. E_{11} and E_{22} are the elastic moduli of the orthotropic material in 1-direction and 2-direction, respectively, G_{12} is the shear modulus, and ν_{12} is Poisson's ratio.

In the same way, the displacement field, Eq. (3), in the notch tip region is also acceptable for the plane V-notch problem of orthotropic material.

In the polar coordinate system $o\rho\theta$, the strain–stress relationships can be written as

$$\left\{ \begin{array}{c} \sigma_{\rho\rho} \\ \sigma_{\theta\theta} \\ \sigma_{\rho\theta} \end{array} \right\} = \left[\begin{array}{ccc} D_{11} & D_{12} & D_{16} \\ D_{12} & D_{22} & D_{26} \\ D_{16} & D_{26} & D_{66} \end{array} \right] \left\{ \begin{array}{c} \varepsilon_{\rho\rho} \\ \varepsilon_{\theta\theta} \\ \varepsilon_{\rho\theta} \end{array} \right\}, \tag{21}$$

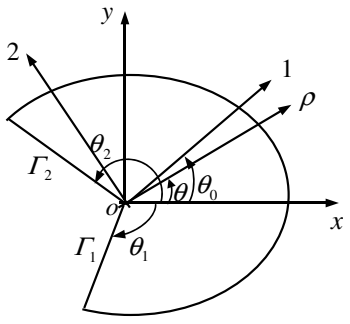

Fig. 4. A V-notch of orthotropic material.

where

$$
\begin{aligned}
D_{11} &= \frac{p_1\cos^4(\bar\theta)+p_2\sin^4(\bar\theta)+2\cos^2(\bar\theta)\sin^2(\bar\theta)(2G_{12}p_3+p_4)}{p_3},\\
D_{12} &= \frac{p_4(\cos^4(\bar\theta)+\sin^4(\bar\theta))+\cos^2(\bar\theta)\sin^2(\bar\theta)(p_1+p_2-4G_{12}p_3)}{p_3},\\
D_{16} &= \cos(\bar\theta)\sin(\bar\theta)\frac{p_1\cos^2(\bar\theta)-p_2\sin^4(\bar\theta)+(\sin^2(\bar\theta)-\cos^2(\bar\theta))(2G_{12}p_3+p_4)}{p_3},\\
D_{22} &= \frac{p_2\cos^4(\bar\theta)+p_1\sin^4(\bar\theta)+2\cos^2(\bar\theta)\sin^2(\bar\theta)(2G_{12}p_3+p_4)}{p_3},\\
D_{26} &= \cos(\bar\theta)\sin(\bar\theta)\frac{p_1\sin^2(\bar\theta)-p_2\cos^4(\bar\theta)-(\sin^2(\bar\theta)-\cos^2(\bar\theta))(2G_{12}p_3+p_4)}{p_3},\\
D_{66} &= \frac{G_{12}p_3(1-4\cos^2(\bar\theta)\sin^2(\bar\theta))+\sin^2(\bar\theta)\cos^2(\bar\theta)(p_1+p_2-2p_4)}{p_3},\\
\bar\theta &= \theta_0-\theta.
\end{aligned}
\tag{22}
$$

For the plane stress problem, there are

$$
p_1=-E_{11}^2,\quad p_2=-E_{11}E_{22},\quad p_3=\upsilon_{12}^2E_{22}-E_{11},\quad p_4=\upsilon_{12}E_{11}E_{22}. \tag{23}
$$

Substitution of Eq. (4) into Eq. (21) yields the stress components as

$$\sigma_{\rho\rho}=\rho^{\lambda}[D_{16}\tilde u'_\rho(\theta)+D_{12}\tilde u'_\theta(\theta)+(D_{11}+D_{12})\tilde u_\rho(\theta)+\lambda(D_{11}\tilde u_\rho(\theta)+D_{16}\tilde u_\theta(\theta))], \tag{24a}$$

$$\sigma_{\theta\theta}=\rho^{\lambda}[D_{26}\tilde u'_\rho(\theta)+D_{22}\tilde u'_\theta(\theta)+(D_{12}+D_{22})\tilde u_\rho(\theta)+\lambda(D_{12}\tilde u_\rho(\theta)+D_{26}\tilde u_\theta(\theta))], \tag{24b}$$

$$\sigma_{\rho\theta}=\rho^{\lambda}[D_{66}\tilde u'_\rho(\theta)+D_{26}\tilde u'_\theta(\theta)+(D_{16}+D_{26})\tilde u_\rho(\theta)+\lambda(D_{16}\tilde u_\rho(\theta)+D_{66}\tilde u_\theta(\theta))]. \tag{24c}$$

According to the same derivations as Section 2, by substituting Eq. (24) into the equilibrium equations Eq. (6) and introducing the two field variables $g_\rho(\theta)$ and $g_\theta(\theta)$, one can obtain the ODE of the plane V-notch problems of orthotropic material as follows:

$$g_\rho=\lambda\tilde u_\rho,\quad \theta\in[\theta_1,\theta_2], \tag{25a}$$

$$g_\theta=\lambda\tilde u_\theta,\quad \theta\in[\theta_1,\theta_2], \tag{25b}$$

$$\begin{aligned}
&D_{66}\tilde u''_\rho+D_{26}\tilde u''_\theta+2D_{16}\tilde u'_\rho+(D_{12}-D_{22})\tilde u'_\theta+(D_{11}-D_{22})\tilde u_\rho+\lambda[2D_{16}\tilde u'_\rho+(D_{12}+D_{66})\tilde u'_\theta+2D_{11}\tilde u_\rho\\
&\quad+(D_{16}-D_{26})\tilde u_\theta]+\lambda[D_{11}g_\rho+D_{16}g_\theta]=0,\quad \theta\in[\theta_1,\theta_2],
\end{aligned} \tag{25c}$$

$$\begin{aligned}
&D_{26}\tilde u''_\rho+D_{22}\tilde u''_\theta+(D_{12}+D_{22}+2D_{66})\tilde u'_\rho+2D_{26}\tilde u'_\theta+2(D_{16}+D_{26})\tilde u_\rho+\lambda[(D_{12}+D_{66})\tilde u'_\rho\\
&\quad+2D_{26}\tilde u'_\theta+(3D_{16}+D_{26})\tilde u_\rho+2D_{66}\tilde u_\theta]+\lambda[D_{16}g_\rho+D_{66}g_\theta]=0,\quad \theta\in[\theta_1,\theta_2].
\end{aligned} \tag{25d}$$

If the traction-free surfaces on Γ_1 and Γ_2 are assumed, introduction of Eq. (24) into Eq. (8) results in the boundary conditions related to the ODE Eq. (25) as follows:

$$D_{26}\tilde u'_\rho+D_{22}\tilde u'_\theta+(D_{12}+D_{22})\tilde u_\rho+\lambda[D_{12}\tilde u_\rho+D_{26}\tilde u_\theta]=0,\quad \theta=\theta_1 \text{ and } \theta_2, \tag{26a}$$

$$D_{66}\tilde u'_\rho+D_{26}\tilde u'_\theta+(D_{16}+D_{26})\tilde u_\rho+\lambda[D_{16}\tilde u_\rho+D_{66}\tilde u_\theta]=0,\quad \theta=\theta_1 \text{ and } \theta_2. \tag{26b}$$

If the V-notch is fixed surface on Γ_1 or Γ_2, the boundary condition can easily be expressed as

$$\tilde u_\rho=0,\quad \theta=\theta_1 \text{ or } \theta_2, \tag{26c}$$

$$\tilde u_\theta=0,\quad \theta=\theta_1 \text{ or } \theta_2. \tag{26d}$$

Hence, the evaluation of the singularity orders λ and the associated eigenfunctions $\tilde u_\rho$ and $\tilde u_\theta$ near the V-notch tip of orthotropic material has been also transformed into solving ODEs Eq. (25) subjected to boundary conditions Eq. (26).

Furthermore, for the solutions of plane V-notch problems of bonded dissimilar multi-material, including the orthotropic materials and anisotropic materials, the same deduction process as shown above can be implemented to compute eigensolutions of the associated ODEs, by which the stress singularity near the V-notch is then determined. This process will produce a set of ODEs that are similar to Eqs. (14)–(16), (18), (20), (25) and (26).

In order to find the solution of the ODEs derived above, in what follows, a numerical method is presented to solve the eigenvalue problems of the ODEs.

5. Interpolating matrix method for solving eigenvalue problems of ODEs

With the development of modern computer techniques, numerical methods have been proposed to solve two-point boundary value problems (BVPs) of ODEs. At present, the most commonly used methods for solving ODEs are the finite difference, shooting and collocation methods. On the basis of the above algorithms, several general-purpose computer routines have been designed as solvers of the BVPs of ODEs. These solvers include PASVA, BOUNDS, SUPORT [29] and COLSYS [30]. The first author [28] established a numerical method by the name of *interpolating matrix method* to solve BVPs of ODEs, by which

the highest derivative appearing in the ODEs is chosen as the unknown parameter of the discrete ODE system. In general, most of the existing methods, including the above mentioned ones, have their own merits and are complementary, depending on the nature of the problems to be solved. However, most of the above solvers deal with two-point BVPs only. To solve the V-notch problems, an efficient method to deal with eigenvalue problems of ODEs is apparently needed. In the present paper, the interpolating matrix method is further developed to solve the above mentioned eigenvalue problems.

Let us consider a set of general linear ODEs, as shown below:

$$\sum_{k=1}^{r}\sum_{j=0}^{m_k} g_{ikj}(x)y_k^{(j)}(x) - \lambda\sum_{k=1}^{r}\sum_{j=0}^{m_k} q_{ikj}(x)y_k^{(j)}(x) = f_i(x), \quad i = 1(1)r, \;\; x \in [a,b] \tag{27}$$

subjected to the following boundary conditions:

$$\sum_{k=1}^{r}\sum_{j=0}^{m_k-1} \alpha_{lkj}y_k^{(j)}(\xi_{lkj}) - \lambda\sum_{k=1}^{r}\sum_{j=0}^{m_k-1} \beta_{lkj}y_k^{(j)}(\xi_{lkj}) = \gamma_l, \quad l = 1(1)t, \;\; a \leqslant \xi_{lkj} \leqslant b, \tag{28}$$

where the symbol $1(1)r$ denotes $1,2,\ldots,r$; $f_i(x)$, $g_{ikj}(x)$ and $q_{ikj}(x) \in c^0[a,b]$ are known functions with respect to x; m_k stands for the highest order of the derivative of each undetermined function $y_k(x)$ in Eq. (27); $y_k^{(j)}$ stands for the jth order derivative of the function $y_k(x)$; $t = \sum_{k=1}^{r} m_k$ is the number of the boundary conditions Eq. (28); α_{lkj}, β_{lkj} and γ_l are known real scalars. ξ_{lkj} can be arbitrary values in the interval $[a,b]$, which express that Eq. (28) can be multi-point boundary conditions. Notice that when $f_i(x)$ and γ_l are identically zero, Eqs. (27) and (28) form an eigenvalue problem of the ODEs, where λ is the associated eigen-parameter.

The interval $[a,b]$ is divided into n subintervals at divisions $a = x_0, x_1, \ldots, x_n = b$. Let $h_i = x_i - x_{i-1}$ be the length of the ith subinterval. Applying Eq. (27) at each of the divisions x_i, $(i = 0,1,\ldots,n)$, results in

$$\sum_{k=1}^{r}\sum_{j=0}^{m_k} \mathbf{G}_{ikj}\mathbf{Y}_k^{(j)}(x) - \lambda\sum_{k=1}^{r}\sum_{j=0}^{m_k} \mathbf{Q}_{ikj}\mathbf{Y}_k^{(j)}(x) = 0, \quad i = 1(1)r, \tag{29}$$

where

$$\begin{aligned}
&\mathbf{G}_{ikj} = \mathrm{diag}(g_{ikj}(x_0), g_{ikj}(x_1), \ldots, g_{ikj}(x_n)),\\
&\mathbf{Q}_{ikj} = \mathrm{diag}(q_{ikj}(x_0), q_{ikj}(x_1), \ldots, q_{ikj}(x_n)),\\
&\mathbf{Y}_k^{(j)}(x) = (y_k^j(x_0), y_k^j(x_1), \ldots, y_k^j(x_n))^{\mathrm{T}}, \quad k = 1(1)r, \;\; j = 0(1)m_k.
\end{aligned}$$

Let $y_{ki}^{(j)}$ denote the approximate values of $y_k^{(j)}(x)$ at x_i, $i = 1(1)n$. The well-known finite difference method takes y_{ki} at the divisions x_i as the basic unknowns of the algebraic equations of the discrete system. Instead, the interpolating matrix method takes $y_{k0}, y'_{k0}, \ldots, y_{k0}^{(m_k-1)}, y_{k0}^{(m_k)}, y_{k1}^{(m_k)}, \ldots, y_{kn}^{(m_k)} (k = 1(1)r)$ as the basic unknowns after discretization. As a result, the $(j-1)$th order derivative of $y_k(x)$ can be expressed in terms of its jth order derivative based on the following integration:

$$y_k^{(j-1)}(x_i) - y_k^{(j-1)}(x_0) = \int_{x_0}^{x_i} y_k^{(j)}(x)\mathrm{d}x, j = 1(1)m_k, k = 1(1)r, i = 1(1)n. \tag{30}$$

Within interval $[a,b]$, $y_k^{(j)}(x)$ can be approximated with the piecewise polynomial interpolation as

$$y_k^{(j)}(x) = \sum_{i=0}^{n} y_k^{(j)}(x_i)L_i(x) + \delta_{kn}^{(j)}(x), \quad x \in [a,b], \tag{31}$$

where $L_i(x)$ are the Lagrangian interpolation polynomials and $\delta_{kn}^{(j)}(x)$ are the residual errors. Introduce the following notations:

$$\omega_{li} = \int_{x_0}^{x_l} L_i(x)\mathrm{d}x, \quad i,l = 0(1)n, \tag{32a}$$

$$\begin{aligned}
&\mathbf{Y}_k(x_0) = (y_k(x_0), y'_k(x_0), \ldots, y_k^{(m_k-1)}(x_0))^{\mathrm{T}}, \quad \mathbf{Y}_{k0} = (y_{k0}, y'_{k0}, \ldots, y_{k0}^{(m_k-1)})^{\mathrm{T}},\\
&\mathbf{Y}_k^{(j)} = (y_{k0}^{(j)}, y_{k1}^{(j)}, \ldots, y_{kn}^{(j)})^{\mathrm{T}}, \quad \sigma = (1,1,\ldots,1)_{(n+1)}^{\mathrm{T}},
\end{aligned} \tag{32b}$$

$$R_{kl}^{(j)} = \int_{x_0}^{x_l} \delta_{kn}^{(j)}(x)\mathrm{d}x, \quad \mathbf{R}_k^{(j)} = (R_{k0}^{(j)}, R_{k1}^{(j)}, \ldots, R_{kn}^{(j)})^{\mathrm{T}}. \tag{32c}$$

Substituting Eq. (31) into (30), and calculating the integrals for $i = 0,1,\ldots,n$, one obtains

$$\mathbf{Y}_k^{(j-1)}(x) = y_k^{(j-1)}(x_0)\boldsymbol{\sigma} + \mathbf{D}\mathbf{Y}_k^{(j)}(x) + \mathbf{R}_k^{(j)}, \quad x \in [a,b]. \tag{33}$$

In Eq. (33), $\mathbf{D} = [\omega_{li}]$ is an $(n+1)\times(n+1)$ matrix whose elements are calculated from the integral in Eq. (32a) and, therefore, called *integral matrix*. For the piecewise linear interpolation, the basis functions in Eq. (31) are

$$L_i(x) = \begin{cases} (x - x_{i-1})/h_i, & x \in [x_{i-1}, x_i],\\ -(x - x_{i+1})/h_{i+1}, & x \in [x_i, x_{i+1}],\\ 0, & \text{others}. \end{cases} \tag{34a}$$

Substituting Eq. (34a) into Eq. (32a) and calculating the integrals ω_{li}, $(i,l = 0(1)n)$, we gain the integral matrix with the linear interpolation which can be written as

$$\mathbf{D} = 0.5\begin{bmatrix} 0 & 0 & \cdots & 0 & 0 \\ 1 & 1 & \cdots & 0 & 0 \\ \vdots & \vdots & \ddots & & \vdots \\ 1 & 1 & \cdots & 1 & 0 \\ 1 & 1 & \cdots & 1 & 1 \end{bmatrix}\begin{bmatrix} 0 & 0 & \cdots & \cdots & 0 \\ h_1 & h_1 & \ddots & & 0 \\ 0 & h_2 & h_2 & \ddots & \vdots \\ \vdots & \ddots & \ddots & \ddots & 0 \\ 0 & \cdots & 0 & h_n & h_n \end{bmatrix}_{(n+1)\times(n+1)} \tag{34b}$$

Thus, for an arbitrary j, the recurrence relation of Eq. (33) results in

$$\mathbf{Y}_k^{(j)}(x) = \mathbf{P}_{kj}\mathbf{Y}_k(x_0) + \mathbf{D}^{m_k-j}\mathbf{Y}_k^{(m_k)}(x) + \mathbf{r}_k^{(j)}, \quad k = 1(1)r,\ j = 1(1)(m_k-1), \tag{35}$$

where

$$\mathbf{r}_k^{(j)} = \sum_{l=0}^{m_k-1-j}[\mathbf{D}^l\mathbf{R}_k^{(j+1+l)}] \tag{36}$$

are the local truncated errors of $\mathbf{Y}_k^{(j)}(x)$, and

$$\mathbf{P}_{kj} = [\overbrace{\mathbf{0},\ldots,\mathbf{0}}^{j},\boldsymbol{\sigma},\mathbf{D}\sigma,\ldots,\mathbf{D}^{m_k-1-j}\boldsymbol{\sigma}]_{(n+1)\times m_k} \tag{37}$$

is an $(n+1)\times m_k$ matrix. Ignoring $\mathbf{r}_k^{(j)}$ in Eq. (35) yields

$$\mathbf{Y}_k^{(j)} = \mathbf{P}_{kj}\mathbf{Y}_{k0} + \mathbf{D}^{m_k-j}\mathbf{Y}_k^{(m_k)}, \quad k = 1(1)r,\ j = 1(1)(m_k-1). \tag{38}$$

It can be seen from Eq. (38) that $\mathbf{Y}_k^{(j)}$ have been represented by $\mathbf{Y}_{k0}$ and $\mathbf{Y}_k^{(m_k)}$. Substituting Eq. (38) into Eq. (29) gives the following algebraic equations:

$$\sum_{k=1}^{r}[\mathbf{A}_{ik}\mathbf{Y}_{k0} + \mathbf{B}_{ik}\mathbf{Y}_k^{(m_k)}] - \lambda\sum_{k=1}^{r}[\mathbf{A}_{\lambda ik}\mathbf{Y}_{k0} + \mathbf{B}_{\lambda ik}\mathbf{Y}_k^{(m_k)}] = \mathbf{0}, \tag{39}$$

where $\mathbf{A}_{ik}$ and $\mathbf{A}_{\lambda ik}$ are $(n+1)\times m_k$ matrices; $\mathbf{B}_{ik}$ and $\mathbf{B}_{\lambda ik}$ are $(n+1)\times(n+1)$ matrices. They are, respectively

$$\mathbf{A}_{ik} = \sum_{j=0}^{m_k-1}\mathbf{G}_{ikj}\mathbf{P}_{kj}, \quad \mathbf{B}_{ik} = \sum_{j=0}^{m_k}\mathbf{G}_{ikj}\mathbf{D}^{m_k-j}, \quad \mathbf{A}_{\lambda ik} = \sum_{j=0}^{m_k-1}\mathbf{Q}_{ikj}\mathbf{P}_{kj}, \quad \mathbf{B}_{\lambda ik} = \sum_{j=0}^{m_k}\mathbf{Q}_{ikj}\mathbf{D}^{m_k-j}. \tag{40}$$

Without loss of generality, consider that the ξ_{lkj} in Eq. (28) take the interval divisions at $x_{I_l}(0 \leqslant I_l \leqslant n)$ within $[a,b]$. In the case of the so-called two-point BVPs, I_l take 0 and n where ξ_{lkj} have the values of a and b. Introducing Eq. (38) into Eq. (28) and letting $\gamma_l = 0$ yield the following eigenvalue problem:

$$\sum_{k=1}^{r}\sum_{j=0}^{m_k-1}\alpha_{lkj}\left[(\mathbf{P}_{kj})_{I_l}\mathbf{Y}_{k0} + (\mathbf{D}^{m_k-j})_{I_l}\mathbf{Y}_k^{(m_k)}\right] - \lambda\sum_{k=1}^{r}\sum_{j=0}^{m_k-1}\beta_{lkj}\left[(\mathbf{P}_{kj})_{I_l}\mathbf{Y}_{k0} + (\mathbf{D}^{m_k-j})_{I_l}\mathbf{Y}_k^{(m_k)}\right] = 0, \tag{41}$$

where $(\mathbf{P}_{kj})_{I_l}$ and $\mathbf{D}_{I_l}$ denote the I_lth row of matrices $\mathbf{P}_{kj}$ and $\mathbf{D}$, respectively. Introducing the following notations into Eq. (41)

$$\mathbf{V}_{\alpha lk} = \sum_{j=0}^{m_k-1}\alpha_{lkj}(\mathbf{P}_{kj})_{I_l}, \quad \mathbf{W}_{\alpha lk} = \sum_{j=0}^{m_k-1}\alpha_{lkj}(\mathbf{D}^{m_k-j})_{I_l}, \tag{42a}$$

$$\mathbf{V}_{\beta lk} = \sum_{j=0}^{m_k-1}\beta_{lkj}(\mathbf{P}_{kj})_{I_l}, \quad \mathbf{W}_{\beta lk} = \sum_{j=0}^{m_k-1}\beta_{lkj}(\mathbf{D}^{m_k-j})_{I_l}, \quad l = 1(1)t \tag{42b}$$

and rewriting the equation, one obtains

$$\sum_{k=1}^{r}(\mathbf{V}_{\alpha lk}\mathbf{Y}_{k0} + \mathbf{W}_{\alpha lk}\mathbf{Y}_k^{(m_k)}) - \lambda\sum_{k=1}^{r}(\mathbf{V}_{\beta lk}\mathbf{Y}_{k0} + \mathbf{W}_{\beta lk}\mathbf{Y}_k^{(m_k)}) = 0. \tag{43}$$

Using the following notations:

$$\mathbf{Y_0} = \begin{Bmatrix} \mathbf{Y}_{10} \\ \mathbf{Y}_{20} \\ \vdots \\ \mathbf{Y}_{r0} \end{Bmatrix}_t, \quad \mathbf{Y} = \begin{Bmatrix} \mathbf{Y}_1^{(m_1)} \\ \mathbf{Y}_2^{(m_2)} \\ \vdots \\ \mathbf{Y}_r^{(m_r)} \end{Bmatrix}_{r(n+1)}, \quad t = \sum_{k=1}^{r}m_k, \tag{44}$$

$$\mathbf{V}_\alpha = [\mathbf{V}_{\alpha lk}]_{t\times t},\quad \mathbf{W}_\alpha = [\mathbf{W}_{\alpha lk}]_{t\times r(n+1)},\quad \mathbf{V}_\beta = [\mathbf{V}_{\beta lk}]_{t\times t},\quad \mathbf{W}_\beta = [\mathbf{W}_{\beta lk}]_{t\times r(n+1)},\quad k = 1(1)r,\qquad l = 1(1)t, \tag{45a}$$

$$\mathbf{A} = [\mathbf{A}_{ik}]_{r(n+1)\times t},\quad \mathbf{B} = [\mathbf{B}_{ik}]_{r(n+1)\times r(n+1)},\quad \mathbf{A}_\lambda = [\mathbf{A}_{\lambda ik}]_{r(n+1)\times t},\quad \mathbf{B}_\lambda = [\mathbf{B}_{\lambda ik}]_{r(n+1)\times r(n+1)},\qquad i,k = 1(1)r \tag{45b}$$

and converting Eqs. (39) and (43) into a combined matrix form, we arrive finally at

$$\begin{bmatrix}\mathbf{V}_\alpha & \mathbf{W}_\alpha\\ \mathbf{A} & \mathbf{B}\end{bmatrix}\begin{Bmatrix}\mathbf{Y}_0\\ \mathbf{Y}\end{Bmatrix} - \lambda\begin{bmatrix}\mathbf{V}_\beta & \mathbf{W}_\beta\\ \mathbf{A}_\lambda & \mathbf{B}_\lambda\end{bmatrix}\begin{Bmatrix}\mathbf{Y}_0\\ \mathbf{Y}\end{Bmatrix} = \mathbf{0}. \tag{46}$$

Eq. (46) is a generalized eigenequation system of $r(n+1)+t$ orders in the unknowns $(\mathbf{Y}_0^{\mathrm{T}}, \mathbf{Y}^{\mathrm{T}})^{\mathrm{T}}$. It can always be converted into a standard eigenvalue formulation through the following transformation:

$$\mathbf{C}_2^{-1}\mathbf{C}_1\begin{Bmatrix}\mathbf{Y}_0\\ \mathbf{Y}\end{Bmatrix} - \lambda\begin{Bmatrix}\mathbf{Y}_0\\ \mathbf{Y}\end{Bmatrix} = \mathbf{0}\quad\text{or}\quad \frac{1}{\lambda}\begin{Bmatrix}\mathbf{Y}_0\\ \mathbf{Y}\end{Bmatrix} - \mathbf{C}_1^{-1}\mathbf{C}_2\begin{Bmatrix}\mathbf{Y}_0\\ \mathbf{Y}\end{Bmatrix} = \mathbf{0}, \tag{47}$$

where

$$\mathbf{C}_1 = \begin{bmatrix}\mathbf{V}_\alpha & \mathbf{W}_\alpha\\ \mathbf{A} & \mathbf{B}\end{bmatrix},\quad \mathbf{C}_2 = \begin{bmatrix}\mathbf{V}_\beta & \mathbf{W}_\beta\\ \mathbf{A}_\lambda & \mathbf{B}_\lambda\end{bmatrix}. \tag{48}$$

Numerical methods from various textbooks about numerical analyses are available to solve the algebraic eigenvalue equations like Eq. (47). In general, the solutions of Eq. (47) provide a finite number of eigenvalues, λ, and the associated eigenvectors $(\mathbf{Y}_0^{\mathrm{T}}, \mathbf{Y}^{\mathrm{T}})^{\mathrm{T}}$. Furthermore the substitution of $(\mathbf{Y}_0^{\mathrm{T}}, \mathbf{Y}^{\mathrm{T}})^{\mathrm{T}}$into Eq. (38) gives the eigenvectors of all the derivatives of $y_k(x)$, i.e. $\mathbf{Y}_k, \mathbf{Y}_k', \ldots, \mathbf{Y}_k^{(m_k-1)}, (k = 1(1)r)$.

It can be seen from the above deduction that the formations of the coefficient matrices in Eq. (47) rely on the integral matrix **D** besides those known functions and parameters in ODEs (27) and (28). In the interpolating matrix method, Eq. (46) or (47) is used to solve the eigenvalue problems of ODEs (27) with the boundary conditions (28), in which the computed error arises from the local truncated errors $\mathbf{r}_k^{(j)}$ in Eq. (35). Thus the accuracy of the interpolating matrix method depends on the integral matrix which represents the influence of a piecewise polynomial interpolation to approximate $y_k^{(j)}(x)$. Generally, the integral matrix **D** with the piecewise quadratic or spline function interpolation is encouraged because of their higher order approximation in comparison with the linear one.

It has been found that for analyzing two-point BVPs of ODEs, in addition to the same some merits as the finite difference and collocation methods, the interpolating matrix method has two distinct advantages as: (1) All functions and their derivatives appearing in the BVPs of ODEs are simultaneously obtained with the same degree of accuracy. This feature is particularly beneficial to the calculation of stress field that requires the first derivative of the displacement functions. (2) It can solve the general eigenvalue problems of ODEs and be convenient to write a general-purpose routine, since the implementary procedure has been expressed as the above unified formulations, especially for the boundary conditions Eq. (28). Moreover, all the solutions corresponding each eigenpair are also obtained with the same degree of accuracy.

According to the above formulations, a general-purpose routine called **IMMEI** is developed in FORTRAN, in which the interpolating matrix method is adopted to solve two-point eigenvalue problem in ODEs expressed in the form of Eqs. (27) and (28).

6. Numerical examples

6.1. Numerical example of solving eigenvalue problems

Before applying the above developed method to V-notch problems, a simple example is shown here to illustrate the effectiveness of the new approach.

Example 1. Bending vibration of a uniform beam hinged at both ends (Fig. 5).

The free vibration equation of the beam is

$$\frac{\mathrm{d}^4Y(x)}{\mathrm{d}x^4} - \beta^4 Y(x) = 0,\quad \beta^4 = \frac{\omega^2 m}{EI},\quad x\in[0,L], \tag{49a}$$

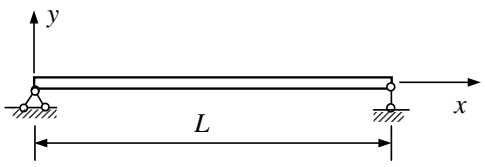

Fig. 5. A simply-supported beam.

where $Y(x)$ is the natural mode of transverse displacement; ω is the natural frequency; L is the length of the beam; EI denotes the flexural rigidity and m the mass per unit length. Here, both EI and m are constant. At the two ends, the boundary conditions are, respectively,

$$Y(0) = 0, \quad Y''(0) = 0, \quad Y(L) = 0, \quad Y''(L) = 0. \tag{49b}$$

$Y(x)$ and ω are determined by solving the eigenvalue problem of Eq. (49), for which exact solutions are available and are

$$\omega_i = (i\pi)^2 \sqrt{\frac{EI}{mL^4}}, \quad i = 1, 2, \ldots, \tag{50a}$$

$$Y_i(x) = A_i \sin \frac{i\pi x}{L}, \tag{50b}$$

where A_i are amplitudes of the mode shapes.

To assess accuracy of the interpolating matrix method (IMMEI), linear and quadratic interpolation functions are used, respectively, to compute the eigenpairs. Here the interval $[0, L]$ is divided into three uniform meshes with the number of subintervals being (n=) 20, 40 and 80, respectively. The solutions of IMMEI in the three meshes are presented to show the convergence rate of the interpolating matrix method as the number of the divisions doubly increases. Table 1 shows the relative errors of the computed eigenvalues ω_i using IMMEI in comparison with the exact solutions. The relative errors of the solutions $Y_i(x), Y_i'(x), Y_i''(x)$ and $Y_i'''(x)$ of the first four modes using IMMEI with the piecewise quadratic **D** and n = 80 are plotted in Figs. 6–9, in turn. In Table 1 and Figs. 6–9, the err% means the relative error defined by below:

$$\text{err}\% = \frac{\text{solution}_{\text{approx}} - \text{solution}_{\text{exact}}}{\text{solution}_{\text{exact}}} \times 100. \tag{51}$$

All of the eigenpairs and their derivatives of various orders of $Y_i(x)$ are simultaneously computed by IMMEI for each mesh. Among them, the computational accuracy of the first eigensolution is highest, whose relative error is about 10^{-5} shown in Table 1 and Fig. 6 when the quadratic **D** with n = 80 is chosen. The accuracy of the solutions is lost gradually for higher modes in the discrete model. Obviously, accuracy can be improved by increasing the number of the divisions of the discrete system. Comparatively, the accuracy using the quadratic **D** is very higher than one using the linear **D** on the same number of the divisions. Many numerical experiments have illustrated that the convergence rates of the present method are about $O(h^4)$ for the quadratic **D** and $O(h^2)$ for the linear **D**, respectively, where h is the length of the subinterval.

Table 1
The natural frequencies $\omega_i(\sqrt{EI/mL^4})$ and the relative errors (%) of the IMMEI solutions

Modes	Exact solutions ω_i	err% of IMMEI with the linear **D**			err% of IMMEI with the quadratic **D**		
		n = 20	n = 40	n = 80	n = 20	n = 40	n = 80
First	π^2	0.4127	0.1029	0.02571	0.001356	0.0001004	0.0000068
Second	$4\pi^2$	1.6682	0.4127	0.1029	0.02183	0.001607	0.000108
Third	$9\pi^2$	3.8210	0.9326	0.2318	0.1116	0.008139	0.000548
Fourth	$16\pi^2$	6.9676	1.6682	0.4127	0.3575	0.02574	0.001733
Fifth	$25\pi^2$	11.257	2.6275	0.6461	0.8873	0.06288	0.004229
Sixth	$36\pi^2$		3.8210	0.9326	1.8773	0.13050	0.008767
Seventh	$49\pi^2$		5.2621	1.2730	3.5648	0.24205	0.01624

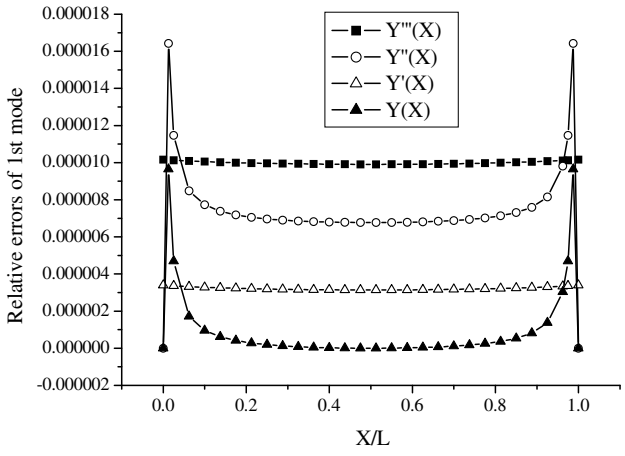

Fig. 6. The computational errors of first mode and its derivatives of higher orders, n = 80.

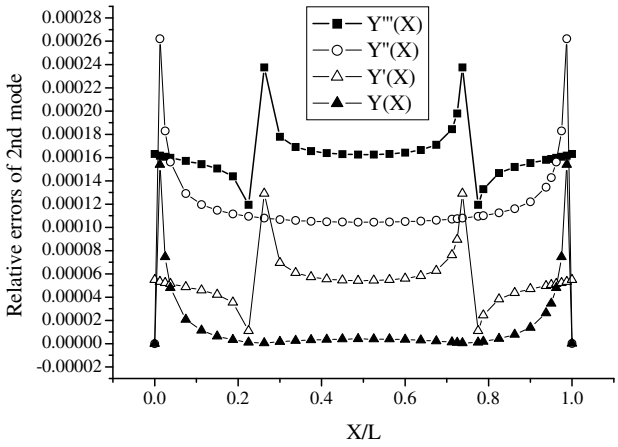

Fig. 7. The computational errors of second mode and its derivatives of higher orders, $n = 80$.

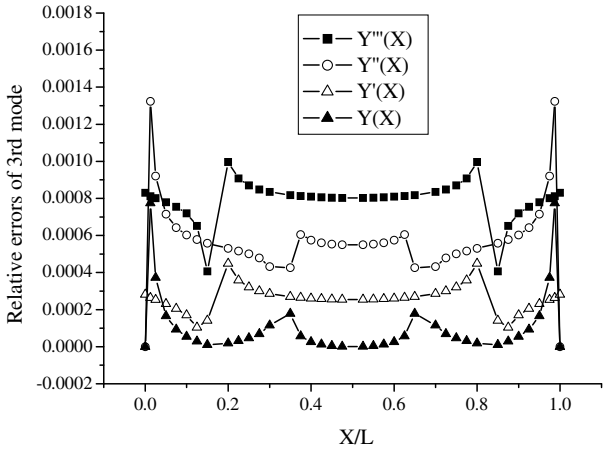

Fig. 8. The computational errors of third mode and its derivatives of higher orders, $n = 80$.

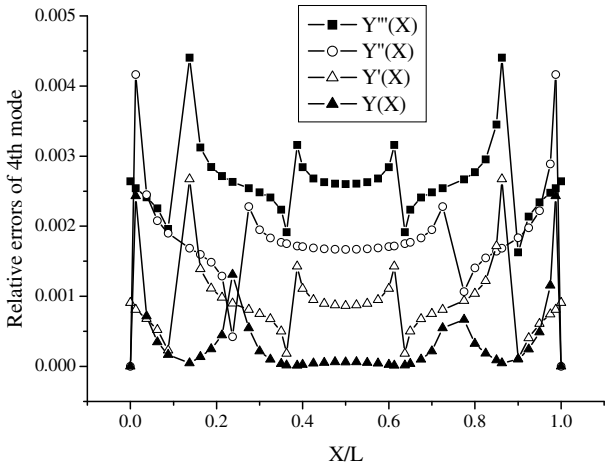

Fig. 9. The computational errors of fourth mode and its derivatives of higher orders, $n = 80$.

In addition, as an advantage of the present method, it can be seen in Table 1 and Figs. 6–9 that all of the solutions $Y_i(x), Y_i'(x), Y_i''(x)$ and $Y_i'''(x)$ for each mode have the same degree of accuracy as the associated natural frequency in terms of their maximum relative errors as comparisons. However, in the finite element and finite difference approaches, the accuracy of the derivatives of higher orders of the modes is lost rapidly because of using the difference.

6.2. Numerical examples of the V-notch problems

This section is concerned with the application of the interpolating matrix method (IMMEI) to the evaluation of the singularity orders of two-dimensional V-notched problems. In the following examples, the integral matrix **D** with quadratic interpolation and uniform division is used in the routine IMMEI.

Example 2. A V-notch of isotropic material as shown in Fig. 2.

The study of the single isotropic V-notch is for the purpose of comparison. Using the sub-region accelerated Müller method, Fu and Long [12] computed a number of eigenvalues of the stress singularity orders of the V-notch problem. Here the routine IMMEI (ab. IMM) is performed to solve the ODEs, (11), (10) and (9) where $\nu = 0.3$ and the opening angle α varies from 0° to 170°. In fact, the computed eigenvalues for the V-notch of a homogeneous isotropic material are independent to Poisson's ratio, while the displacement eigenfunctions and ν are related. For each given α, interval $[\theta_1, \theta_2]$ are divided into three uniform meshes with $n = 20$, 40 and 80, respectively, where the interval implies a circle arc from θ_1 to θ_2 with a radius ρ at the V-notch tip. The newly computed results are given in Tables 2 and 3, where n is the number of the divisions within interval $[\theta_1, \theta_2]$. The eigenvalues λ are usually complex and are expressed by $\lambda_k = \xi_k + i\eta_k$ where $i = \sqrt{-1}$. Obviously, if the imaginary part η_k is equal to zero, λ_k is real. One of the useful features of IMMEI is that all the small eigenvalues beyond $\xi_k \geqslant -1$ and their eigenvectors are determined simultaneously. Notice that $\lambda_k = -1$ is always a four-time repeated eigenvalue for all of the two-dimensional V-notch problems. There are two different eigenvectors associated with $\lambda_k = -1$. When the two eigenpairs associated with $\lambda_k = -1$ are introduced into Eq. (3), it can be found that the corresponding terms in Eq. (3) represent two components of the rigid translation of the structures. Thus, this special eigenvalue is not included in Tables 2 and 3. In addition, another component of the rigid translation is referred to the term of $\lambda_k = 0$ in Eq. (3). Table 2 lists the eigenvalues related to the symmetrical displacement (mode I) eigenfunction $\tilde{u}_\rho(\theta)$ and Table 3 lists those related to the anti-symmetrical displacement (mode II) eigenfunction $\tilde{u}_\rho(\theta)$. In the case $\alpha = 60°$, the results of Ref. [26] were obtained using the special FEM by means of three leading terms of the analytical constrains of the stress field, where the half of the notch structure, due to symmetry conditions, was discretized with 152 six-node triangular elements.

Table 2
The eigenvalues corresponding to the symmetrical displacement eigenfunction $\tilde{u}_\rho(\theta)$

α	Methods	ξ_1	η_1	ξ_2	η_2	ξ_3	η_3	ξ_4	η_4
170°	Ref. [12]	−0.099956	0	1.001795	0	1.695232	0	3.022680	0
	IMM, $n = 20$	−0.0997671	0	1.000629	0	1.706359	0	2.972986	0
	IMM, $n = 40$	−0.099949	0	1.001733	0	1.695693	0	3.020562	0
	IMM, $n = 80$	−0.099955	0	1.001789	0	1.695286	0	3.022390	0
150°	Ref. [12]	−0.248025	0	1.106286	0.096100	2.828294	0.347177	4.547288	0.459268
	IMM, $n = 20$	−0.247871	0	1.109776	0.087307	2.859206	0.321400	4.705928	0.308320
	IMM, $n = 40$	−0.248019	0	1.106531	0.095588	2.830449	0.345590	4.556639	0.452879
	IMM, $n = 80$	−0.248025	0	1.106303	0.0960594	2.828434	0.347070	4.547904	0.458893
120°	Ref. [12]	−0.384269	0	0.833549	0.252251	2.343717	0.414037	3.849458	0.506015
	IMM, $n = 20$	−0.384138	0	0.836062	0.252153	2.365450	0.414282	3.957761	0.498516
	IMM, $n = 40$	−0.384259	0	0.833734	0.252249	2.345190	0.414126	3.856164	0.506382
	IMM, $n = 80$	−0.384268	0	0.833561	0.252251	2.343817	0.414042	3.849910	0.506043
90°	Ref. [12]	−0.455516	0	0.629257	0.231251	1.971844	0.373931	3.310377	0.455494
	IMM, $n = 20$	−0.455395	0	0.631172	0.232519	1.988336	0.383516	3.394304	0.488602
	IMM, $n = 40$	−0.455511	0	0.629323	0.231332	1.972392	0.374414	3.313047	0.457263
	IMM, $n = 80$	−0.455516	0	0.629267	0.231257	1.971920	0.373979	3.310732	0.455687
60°	Ref. [12]	−0.487779	0	0.471028	0.141853	1.677615	0.284901	2.881487	0.360496
	Ref. [26]	−0.4878	0	0.4710	0.1418	1.6776	0.2849		
	IMM, $n = 20$	−0.487717	0	0.471813	0.143640	1.684805	0.296623	2.924016	0.408020
	IMM, $n = 40$	−0.487775	0	0.471073	0.141991	1.678017	0.285650	2.883292	0.363632
	IMM, $n = 80$	−0.487778	0	0.471035	0.141869	1.677673	0.284994	2.881766	0.360853
30°	Ref. [12]	−0.498547	0	0.202957	0	0.490378	0	1.440492	0.114207
	IMM, $n = 20$	−0.498472	0	0.205806	0	0.488633	0	1.445210	0.147248
	IMM, $n = 40$	−0.498540	0	0.205806	0	0.490268	0	1.440740	0.116222
	IMM, $n = 80$	−0.498546	0	0.202983	0	0.490363	0	1.440530	0.114502
10°	Ref. [12]	−0.499947	0	0.058843	0	0.499728	0	1.118823	0
	IMM, $n = 20$	−0.499856	0	0.060933	0	0.498345	0	1.151176	0
	IMM, $n = 40$	−0.499934	0	0.059126	0	0.499521	0	1.122380	0
	IMM, $n = 80$	−0.499946	0	0.058862	0	0.499716	0	1.119061	0
0°	Exact solutions	−0.50000	0	0	0	0.50000	0	1.00000	0
	IMM, $n = 20$	−.499794	0	0.003578	0	0.497325	0	1.043821	0
	IMM, $n = 40$	−.499985	0	0.000257	0	0.499804	0	1.002930	0
	IMM, $n = 80$	−.499999	0	0.000017	0	0.499987	0	1.000197	0

Table 3
The eigenvalues corresponding to the anti-symmetrical displacement eigenfunction $\tilde{u}_\rho(\theta)$

α	Methods	ξ_1	η_1	ξ_2	η_2	ξ_3	η_3	ξ_4	η_4	ξ_5	η_5
170°	Ref. [12]	0.798933	0	0	0	2.007826	0	2.586721	0	4.060480	0
	IMM, $n = 20$	0.800916	0	0	0	1.997193	0	2.631530	0	3.902388	0
	IMM, $n = 40$	0.799004	0	0	0	2.007389	0	2.588412	0	4.048878	0
	IMM, $n = 80$	0.798942	0	0	0	2.007772	0	2.586934	0	4.058970	0
150°	Ref. [12]	0.485814	0	0	0	1.967836	0.261186	3.688038	0.409575	5.406179	0.500793
	IMM, $n = 20$	0.487279	0	0	0	1.979418	0.249763	3.760510	0.349527	5.467941	0
	IMM, $n = 40$	0.485919	0	0	0	1.968624	0.260421	3.692685	0.406489	5.422865	0.490318
	IMM, $n = 80$	0.485819	0	0	0	1.967891	0.261135	3.688348	0.409368	5.407307	0.500164
120°	Ref. [12]	0.148913	0	0	0	1.589479	0.348375	3.090928	0.464641	4.601514	0.541087
	IMM, $n = 20$	0.150009	0	0	0	1.597549	0.348528	3.147310	0.463943	4.820487	0.503578
	IMM, $n = 40$	0.148992	0	0	0	1.590100	0.348397	3.100330	0.464789	4.614583	0.541504
	IMM, $n = 80$	0.148918	0	0	0	1.589517	0.348376	3.097151	0.464653	4.602357	0.541143
90°	Ref. [12]	−0.091471	0	0	0	1.301327	0.315838	2.641420	0.418787	3.978902	0.486625
	IMM, $n = 20$	−0.090574	0	0	0	1.307470	0.319829	2.680315	0.437987	4.148389	0.532426
	IMM, $n = 40$	−0.091436	0	0	0	1.301562	0.315956	2.642884	0.419538	3.984719	0.489385
	IMM, $n = 80$	−0.091466	0	0	0	1.301356	0.315856	2.641593	0.418888	3.979574	0.486968
60°	Ref. [12]	−0.269099	0	0	0	1.074826	0.229426	2.279767	0.326690	3.482900	0.388984
	Ref. [26]	−0.2691	0	0	0	1.0749	0.2294				
	IMM, $n = 20$	−0.268710	0	0	0	1.077382	0.234207	2.297998	0.351998	3.574251	0.469510
	IMM, $n = 40$	−0.269070	0	0	0	1.075014	0.229741	2.280884	0.328306	3.487289	0.394444
	IMM, $n = 80$	−0.269095	0	0	0	1.074848	0.229466	2.279900	0.326881	3.483436	0.389603
30°	Ref. [12]	−0.401808	0	0	0	0.838934	0	0.948560	0	1.987005	0.166741
	IMM, $n = 20$	−0.401460	0	0	0	0.881197	0	0.909578	0	1.999550	0.222443
	IMM, $n = 40$	−0.401781	0	0	0	0.840591	0	0.947180	0	1.987897	0.170364
	IMM, $n = 80$	−0.401805	0	0	0	0.839163	0	0.948357	0	1.987095	0.167222
10°	Ref. [12]	−0.470645	0	0	0	0.588609	0	0.999107	0	1.649700	0
	IMM, $n = 20$	−0.470319	0	0	0	0.597760	0	0.991337	0	1.770116	0
	IMM, $n = 40$	−0.470599	0	0	0	0.589736	0	0.998226	0	1.659348	0
	IMM, $n = 80$	−0.470642	0	0	0	0.588685	0	0.999045	0	1.650330	0
0°	Exact solutions	−0.50000	0	0	0	0.500000	0	1.000000	0	1.50000	0
	IMM, $n = 20$	−0.499373	0	0	0	0.513993	0	0.987129	0	1.62522	0
	IMM, $n = 40$	−0.499954	0	0	0	0.500983	0	0.999039	0	1.50741	0
	IMM, $n = 80$	−0.499997	0	0	0	0.500066	0	0.999935	0	1.50049	0

Tables 2 and 3 show that the eigenvalues obtained using the present method approach the results of Ref. [12] as n increases. In the tables, the two eigenvalues in the range of $-1 < \lambda_k < 0$ for $n = 40$ have converged up to the fourth significant figure. It is found that there exists either one or two real eigenvalues when $0 \leqslant \alpha < 180°$ for the V-notch of isotropic material. In this study, the eigenvalues whose real parts are between -1 and 0, i.e. $\mathrm{Re}(\lambda) \in (-1, 0)$, are the important parameters that are directly related to the singularity order of the stress field at the V-notch tip. In addition, some eigenvalues when $\mathrm{Re}(\lambda) \geqslant 0$ should be also considered if the near tip stress field is determined.

The highest order of singularity is -0.5 for both mode I and mode II occurring at $\alpha = 0$, i.e. for a line crack. For the crack problem, all the exact eigenvalues can be predicted to be real and take $-1 + 0.5k$, $k = 0, 1, 2, \ldots$ It is well known in the finite element analysis that the "quarter-point" element [31,32] at crack tip can efficiently model the singular stress field near the crack tip, in which the mid-side nodes near the crack tip are placed at the quarter point. In fact, the element at crack tip assumes the following stress mode:

$$\sigma_{ij} = \frac{a_{ij}}{\sqrt{\rho}} + b_{ij} + c_{ij}\sqrt{\rho}, \tag{52}$$

which coincides with the stress field related to the first three eigenvalues -0.5, 0 and 0.5. However, it can be seen in Tables 2 and 3 that shape function Eq. (52) of the quarter-point element is no longer available to modeling the stress field near the V-notch tips of the cases $\alpha > 10°$, at least, because the singularity orders here are not -0.5 and 0.5.

Example 3. A V-notch of bonded dissimilar bimaterial as shown in Fig. 3.

The V-notch consists of two different isotropic materials and is a plane strain problem. The bonded interface lies at $\theta = \theta_2$. The opining angle is $(\theta_3 - \theta_1)$. Poisson's ratios of the materials are $\nu_1 = 0.167$ and $\nu_2 = 0.210$, respectively. In the parametric study, E_2/E_1 is variable. Refs. [13,5] used Newton's iteration to calculate the stress singularities through an eigenequation derived by using complex functions. The two intervals $[\theta_1, \theta_2]$ and $[\theta_2, \theta_3]$ are divided into the same number of subintervals with equal segment in each interval. In the tables, n is the number of the divisions within each interval and $\lambda_k = \xi_k + \mathrm{i}\eta_k$ is the same meaning to Example 2. Due to the lack of exact solutions for comparisons, very fine divisions are adopted for the V-notch with $E_2/E_1 = 0.5$, $\theta_1 = 0°$, $\theta_2 = 90°$ and $\theta_3 = 270°$. The results using IMMEI with finer mesh of $n = 160$ are acted as

Table 4
The eigenvalues of the V-notch with $\theta_1 = 0°$, $\theta_2 = 90°$, $\theta_3 = 270°$, $E_1/E_2 = 2$

Methods	ξ_1	η_1	ξ_2	η_2	ξ_4	η_4	ξ_5	η_5	ξ_6	η_6
Ref. [5]	−0.488	0								
Ref. [13]	−0.48756	0	−0.16731	0						
IMM, $n = 10$	−0.4873683	0	−0.1663428	0	0.5784164	0.1962388	1.4616128	0.2663404	1.8648616	0.6727592
IMM, $n = 20$	−0.4875405	0	−0.1672198	0	0.5752737	0.1949118	1.4440259	0.2566424	1.8589506	0.6695227
IMM, $n = 40$	−0.4875569	0	−0.1673009	0	0.5750053	0.1948013	1.4426988	0.2558552	1.8585303	0.6692342
IMM, $n = 80$	−0.4875581	0	−0.1673069	0	0.5749855	0.1947932	1.4426019	0.2557975	1.8584998	0.6692129
IMM, $n = 160$	−0.4875582	0	−0.1673073	0	0.5749842	0.1947926	1.4425954	0.2557936	1.8584977	0.6692115

Note: $\xi_3 = 0$, $\eta_3 = 0$ for all of the above models.

Table 5
The eigenvalues of the V-notch with $\theta_1 = 0°$, $\theta_2 = 90°$, $\theta_3 = 270°$

E_2/E_1	Ref. [5]	Ref. [13]		IMMEI					
				$n = 20$		$n = 40$		$n = 80$	
	λ_1	λ_1	λ_2	λ_1	λ_2	λ_1	λ_2	λ_1	λ_2
0.33	−0.498	−0.49805	−0.22194	−0.4980360	−0.2218669	−0.4980532	−0.2219326	−0.4980545	−0.2219375
0.5	−0.488	−0.48756	−0.16731	−0.4875405	−0.1672198	−0.4875569	−0.1673009	−0.4875581	−0.1673069
1.0	−0.450	−0.45074	−0.09252	−0.4507273	−0.0923977	−0.4507428	−0.0925077	−0.4507440	−0.0925159
2.14	−0.390	−0.39034	−0.04170	−0.3903270	−0.0415509	−0.3903419	−0.0416890	−0.3903430	−0.0416992
4.0	−0.337	−0.33611	−0.01944	−0.3360963	−0.0192742	−0.3361104	−0.0194300	−0.3361115	−0.0194415
10.0	−0.270	−0.26966	−0.00529	−0.2696441	−0.0051051	−0.2696558	−0.0052800	−0.2696567	−0.0052930

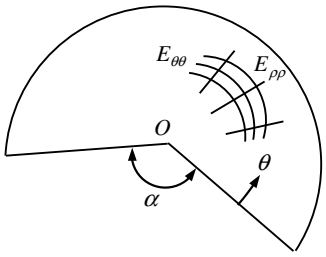

Fig. 10. The V-notch of orthotropic material.

the standard solution shown in Table 4. It is seen in Table 4 that the first six eigenvalues yielded by taking $n = 80$ and $n = 160$ agree with each other up to the sixth significant figure. Thus, the computed results using IMMEI in Table 5 are obtained by taking up to $n = 80$ only. In general cases of the bimaterial V-notch of isotropic material, there exist two real eigenvalues in the range of $-1 < \lambda_k < 0$. It can be seen in Tables 4 and 5 that the IMMEI solutions converge and agree well with the alternative numerical results. Thus, in Tables 4 and 5, the solutions of IMMEI are always given to show convergence rate of the algorithm with respect to the division refinement and comparisons with the results from Refs. [13,5]. In general, Tables 4 and 5 show that IMMEI can provide very accurate results. For instance, apart from the very small imaginary components, all the results in Table 5 obtained using IMMEI with $n = 40$ are converged up to the fifth significant figure. Furthermore all the associated eigenvectors are computed with the same degree of accuracy.

Example 4. A plane V-notch of orthotropic material as shown in Fig. 10.

The V-notch of orthotropic material is a plane stress problem. The opining angle is α. Two principal axes of the material are along ρ-direction and θ-direction related to the polar coordinate system, respectively. $E_{\theta\theta}$,$E_{\rho\rho}$ are the hoop and radial elastic moduli, respectively, $\mu_{\rho\theta}$ the Poisson's ratio, $G_{\rho\theta}$ the shear modulus. Let $E_{\theta\theta}/E_{\rho\rho} = 0.0375$, $G_{\rho\theta}/E_{\rho\rho} = 0.1$, $\mu_{\rho\theta} = 0.187$.

Evidently, the stress singularity orders and the stress fields near the notch roots vary as the change of α. Delale et al. [33] given an analytic solution for the stress singularity orders. Pageau et al. [6] used the finite element method to achieve the numerical results for it. Here IMMEI is employed to solve the ODEs Eqs. (31) and (32) in order to determine the stress singularity orders for several different opening angles. The computed results of λ_1 are shown in Tables 6 and 7, where n is the number of the divisions. Notice that even if $\alpha > 180°$, there exist the stress singularity orders within $\lambda_i \in (-1,0)$ for the orthotropic material. In fact, the number of the stress singularity orders within $\lambda_i \in (-1,0)$ increases as the decrease of the opening angle α. When $\alpha = 0$, the number of λ_i within $(-1,0)$ is maximum, where there are five stress singularity orders for the above values of the material parameters. And the first five stress singularity orders, λ_i, are all real roots in the case as

Table 6
λ_1 of the V-notch of the orthotropic material in several different α

α	IMMEI, $n = 20$	IMMEI, $n = 40$	IMMEI, $n = 80$	IMMEI, $n = 160$	Ref. [6], FEM	Ref. [33], Analytic solution
240°	−0.2848977	−0.2850110	−0.2850194	−0.2850200	−0.284846	−0.285032
180°	−0.6897694	−0.6898106	−0.6898137	−0.6898139	−0.689715	−0.689816
120°	−0.8129647	−0.8129932	−0.8129953	−0.8129954	−0.812902	−0.812996
60°	−0.8492186	−0.8492432	−0.8492450	−0.8492452	−0.849159	−0.849246
0°	−0.8555746	−0.8556059	−0.8556082	−0.8556084	−0.855492	−0.855608

Table 7
The first five λ_i for the V-notch of the orthotropic material when $\alpha = 0°$

	IMMEI, $n = 20$	IMMEI, $n = 40$	IMMEI, $n = 80$	IMMEI, $n = 160$	Ref. [6], FEM	Ref. [33], Analytic solution
λ_1	−0.8555746	−0.8556059	−0.8556082	−0.8556084	−0.855607	−0.855608
λ_2	−0.8348093	−0.8349901	−0.8350034	−0.8350043	−0.834996	−0.835006
λ_3	−0.6646219	−0.6655667	−0.6656353	−0.6656399	−0.665614	−0.665643
λ_4	−0.4545949	−0.4581610	−0.4584159	−0.4584331	−0.458360	−0.458441
λ_5	−0.2141988	−0.2251511	−0.2259155	−0.2259670	−0.225788	−0.225985

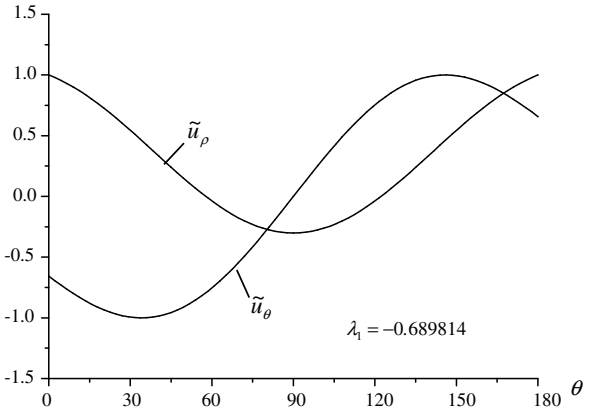

Fig. 11. Displacement eigenvectors of the V-notch when $\alpha = 180°$, $n = 80$.

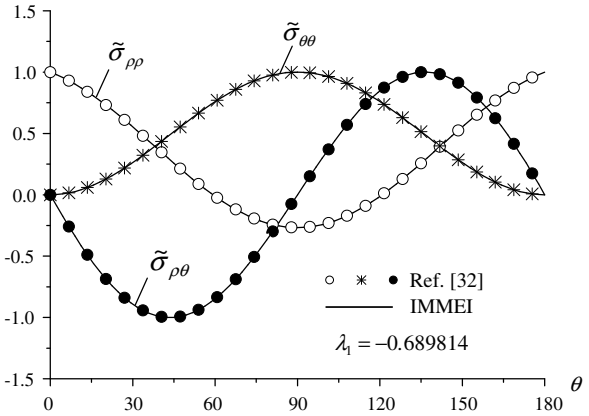

Fig. 12. Stress eigenvectors of the V-notch when $\alpha = 180°$, $n = 80$.

shown in Table 7. In Table 6, it is seen that the computed λ_1 using IMMEI with $n = 80$ are converged up to the sixth significant figure in contrast to the results of IMMEI with $n = 160$ and Refs. [33,6]. In addition, all the associated eigenvectors are achieved with the same degree of accuracy. As a result, the angular distribution functions $\tilde{u}_\rho(\theta)$, $\tilde{u}_\theta(\theta)$, $\tilde{\sigma}_{\rho\rho}(\theta)$, $\tilde{\sigma}_{\theta\theta}(\theta)$ and $\tilde{\sigma}_{\rho\theta}(\theta)$ associated with λ_1 when $\alpha = 180°$ and taking $n = 80$ are plotted in Figs. 11 and 12, respectively. It is seen in Fig. 12 that the stress angular distribution functions using IMMEI are in good agreement with ones from Ref. [33].

7. Conclusions

By assuming an asymptotic stress field, the governing differential equations of linear elasticity in the notch tip region were transformed into a general eigenvalue problem of ordinary differential equations (ODEs), the solution of which provided the singularity orders at plane V-notch tips. The interpolating matrix method was further developed to solve the general eigenvalue problem. One of the unique features of the interpolating matrix method is that the method takes $y_{k0}, y'_{k0}, \ldots, y_{k0}^{(m_k-1)}, y_{k0}^{(m_k)}, y_{k1}^{(m_k)}, \ldots, y_{kn}^{(m_k)}$, $(k = 1(1)r)$, as the fundamental unknowns of the algebraic equation system after discretization, which include the highest derivatives of all functions appearing in the fundamental equations. According to the formulations of the interpolating matrix method, the new solver called IMMEI was developed in FORTRAN, which is adopted to solve the general eigenvalue problem in ODEs. By following the solution procedure, the main singularity orders of plane V-notches are calculated from solving the eigenvalue problems of the ODEs. In parallel, the associated eigenvectors of the displacement and stress fields near the V-notches are also determined.

The applications of the present method in terms of determining the stress singularities for general plane V-notch problems have the following features: (1) The number of wedges can be arbitrary; (2) Each wedge can be any kind of anisotropic materials; (3) Each wedge angle can be arbitrary; (4) The boundary conditions of the V-notch can be free–free, free–fixed and fixed–fixed; (5) All of the useful main stress singularity orders and the associated eigenvectors are simultaneously obtained by implementing the interpolating matrix method to the governing ordinary differential equations (ODEs) of V-notches, because the ODEs and the derived algebraic eigenequations are linear. One obvious advantage is that the solutions of each eigenvalue and the associated eigenfunctions as well as their derivatives are simultaneously computed with the same degree of accuracy. Especially, these accurate eigenvectors and their derivatives near the V-notch tip are needed in the analysis of the near tip stress field and the notch stress intensity factors.

Numerical examples have been given to show the applications of the present method. Comparisons with the results in the literatures were made and have shown that the new method is an effective and accurate tool for dealing with singularity orders of general plane V-notches.

Acknowledgements

The work was supported by the Doctorial Program Foundation of the Ministry of Education (20050359009) and the Natural Science Foundation of Anhui Province (050440503), PR China.

References

[1] M.L. Williams, Stress singularities resulting from various boundary conditions in angular corners of plates in tension, J. Appl. Mech. 19 (1952) 526–528.
[2] M.L. Williams, On the stress distribution at the base of stationary crack, J. Appl. Mech. 24 (1957) 109–114.
[3] M.C. Chen, K.Y. Sze, A novel finite element analysis of bimaterial wedge problems, Eng. Fract. Mech. 68 (2001) 1463–1476.
[4] Z. Yosibash, B.A. Szabó, A note on numerically computed eigenfunctions and generalized stress intensity factors associated with singular points, Eng. Fract. Mech. 54 (1996) 593–595.
[5] D.B. Bogy, Two edge-bonded elastic wedges of different materials and angles under surface traction, J. Appl. Mech. 38 (2) (1971) 377–386.
[6] S.S. Pageau, P.F. Joseph, S.B. Biggers, Finite element analysis of anisotropic materials with singular inplane stress fields, Int. J. Solids Struct. 32 (1995) 571–591.
[7] B. Gross, J.E. Srawley, W.F. Brown, Stress intensity factors for a singular-edge-notch tension specimen by boundary collocation, NASA TN D-2395, 1964.
[8] B. Gross, A. Mendelson, Plane elastic analysis of V-notched plates, Int. J. Fract. Mech. 8 (1972) 267–276.
[9] W.C. Carpenter, The eigenvector solution for a general corner or finite opening crack with further studies on the collocation procedure, Int. J. Fract. 27 (1985) 63–74.
[10] W. Rzasnicki, A. Mendelson, L.U. Albers, Application of boundary integral method to elastoplastic analysis of V-notched beams, Int. J. Fract. 11 (1975) 329–342.
[11] C.L. Tan, Y.L. Gao, F.F. Afagh, Boundary element analysis of interface cracks between dissimilar anisotropic materials, Int. J. Solids Struct. 29 (1992) 3201–3220.
[12] X.R. Fu, Y.U. Long, Analysis of plane notch problems with analytical trial functions' method, Eng. Mech. 20 (4) (2003) 33–38. 73 (in Chinese).
[13] Z. Jian, S.H. Huang, L.M. Hu, Computation of stress factors for bimaterial V-notch and heel of concrete dam on rock foundation, Chin. J. Hydraul. Eng. 6 (1998) 77–81 (in Chinese).
[14] K.S. Gadi, P.F. Joseph, N.S. Zhang, A.C. Kaya, Thermally induced logarithmic stress singularities in a composite wedge and other anomalies, Eng. Fract. Mech. 65 (2000) 645–664.
[15] J. Li, X.B. Zhang, N. Recho, Stress singularities near a tip of a two-dimensional notch formed from several elastic anisotropic materials, Int. J. Fract. 107 (4) (2001) 379–395.
[16] A.N. Stroh, Dislocations and cracks in anisotropic elasticity, Philos. Mag. 3 (1958) 625–646.
[17] T.C.T. Ting, Anisotropic Elasticity: Theory and Applications, Oxford University Press, 1996.
[18] T.C.T. Ting, Stress singularities at the tip of interfaces in polycrystals, in: H.P. Rossmanith (Ed.), Damage and Failure of Interfaces, Balkema, Rotterdam, Netherlands, 1997, pp. 75–82.
[19] C. Hwu, M. Omiya, K. Kishimoto, A key matrix *N* for the stress singularity of the anisotropic elastic composite wedges, JSME Int. J. Ser. A 46 (2003) 40–50.
[20] P.E.W. Labossiere, M.L. Dunn, Stress intensities at interface corners in anisotropic bimaterials, Eng. Fract. Mech. 62 (1999) 555–575.
[21] C. Hwu, T.L. Kuo, A unified definition for stress intensity factors of interface corners and cracks, Int. J. Solids Struct. 44 (2007) 6340–6359.
[22] M. Stern, E.B. Becker, R.S. Dunham, A contour integral computation of mixed-mode stress intensity factors, Int. J. Fract. 12 (3) (1976) 359–368.
[23] C.H. Chue, C.I. Liu, A general solution on stress singularities in an anisotropic wedge, Int. J. Solids Struct. 28 (2001) 6889–6906.
[24] H.M. Wigger, W. Becker, Inplane stress singularities at the interface corner of a bimaterial junction, Compos. Struct. 69 (2005) 193–199.
[25] W.C. Sue, J.Y. Liou, J.C. Sung, Investigation of the stress singularity of a magnetoelectroelastic bonded antiplane wedge, Appl. Math. Modell. 31 (2007) 2313–2331.
[26] A. Seweryn, Modeling of singular stress fields using finite element method, Int. J. Solids Struct. 39 (2002) 4787–4804.

[27] A. Carpinteri, M. Paggi, N. Pugno, Numerical evaluation of generalized stress-intensity factors in multi-layered composites, Int. J. Solids Struct. 43 (2006) 627–641.
[28] Z.R. Niu, Nonlinear bending of the shallow spherical shells with variable thickness under axisymmetrical loads, Appl. Math. Mech. 14 (11) (1993) 1023–1031.
[29] I. Gladwell, A survey of subroutine for solving BVPs in ODEs, in: Proceedings on Computational Techniques for ODEs, A.P. Inc, 1980. pp. 273–303.
[30] U. Ascher, J. Christiansen, R.D. Russel, Algorithm 569, COLSYS: collocation software for boundary value ODEs [D2], Math. Software 7 (1981) 223–229.
[31] R.D. Henshel, K.G. Shaw, Crack tip finite elements are unnecessary, Int. J. Numer. Methods Eng. 9 (1976) 495–507.
[32] R.S. Barsoum, On the use of isoparametric finite elements in linear fracture mechanics, Int. J. Numer. Methods Eng. 10 (1976) 25–27.
[33] F. Delale, F. Erdogan, H. Bodurogul, Stress singularities at the vertex of a cylindrically at isotropic wedge, Int. J. Fract. 19 (1982) 247–256.